J Electroceram (2006) 16: 179–186
DOI 10.1007/s10832-006-6203-x

Cuprate-ferrate compositions for temperature independent resistive oxygen sensors

Kathy Sahner · Jochen Straub · Ralf Moos

Received: 25 May 2005 / Revised: 7 September 2005 / Accepted: 11 November 2005

Abstract In this contribution, the binary ceramic system La_2CuO_4-$LaFeO_3$ is investigated for resistive oxygen sensor applications. The temperature-independent characteristics that are observed for copper contents of 30% or higher are of particular interest. In order to correlate sensor characteristics and material composition, an initial model describing the complex two-phase system is proposed. It is based on the so-called generalized effective media theory (GEMT), a useful tool for describing bi-phase composites. The fitting procedure allows to predict the actual sensor characteristics determined by the experiments.

Keywords Perovskite · Generalized effective media theory · Lanthanum cuprate · Lanthanum ferrate · Strontium titanate

Introduction

In order to control engine operation, nearly every passenger car powered by a gasoline engine is equipped with at least one oxygen sensor measuring the air-to-fuel ratio. State-of-the-art for such lambda probes are solid state potentiometric electrolyte sensors based upon yttrium stabilized zirconia (YSZ) [1], which are manufactured in a multi-layer technique by tape casting and hybrid technology similar to the manufacturing of electronic thick film circuits. Although such devices present fast and stable response characteristics, the potential of resistive semiconductor systems has been investigated in order to reduce the manufacturing costs. Due to their simple design, resistive oxygen sensors based on materials such as TiO_2 [2], $SrTiO_3$ [3] and CeO_2 [4, 5] are expected to be an inexpensive alternative to the zirconia-based combined amperometric-potentiometric wideband lambda probes, which present a complex set-up. Although the oxygen sensitivity of these resistive sensors is sufficient, a major drawback for practical application is the pronounced temperature interference observed for resistive sensor devices. For upcoming sensor generations, fast response and temperature independent sensor characteristics are of high interest. In order to decrease the temperature dependence of the sensor output, the use of an additional temperature compensating material has been investigated [6–8]. Another approach is the use of a sensitive material presenting an intrinsic temperature independent conductivity. Among the first examples of such materials, $BaTa_{0.8}Fe_{0.2}O_3$ [9], La-doped $SrTi_{1-y}Fe_yO_{3-\delta}$ [10, 11] and La_2CuO_4 [12] have been reported in the literature. The latter is known for its excellent temperature independent properties [12]. However, the material is not stable at high temperatures and under reducing conditions [13].

As yet another semiconductor system, the perovskite-like lanthanum ferrate $LaFeO_3$ has been studied [14]. Although this material was not found to present interesting oxygen sensing characteristics, its chemical stability is excellent. A previous study therefore aimed at combining the complementary advantages of $LaFeO_3$ and La_2CuO_4 [15, 16]. After a partial substitution of iron in the $LaFeO_3$ lattice with copper, oxygen sensitivity as well as temperature independency were improved without deteriorating thermal and chemical stability. In this case, the resulting material was assumed to present the formula $LaCu_xFe_{1-x}O_3$. At low copper contents, i.e. at low values of x, an improved stability was observed toward sensor poisons such as sulfur dioxide. Figure 1 presents the output of several porous thick film

K. Sahner (✉) · J. Straub · R. Moos
Functional Materials, University of Bayreuth, 95440 Bayreuth, Germany
e-mail: Functional.Materials@Uni-Bayreuth.de

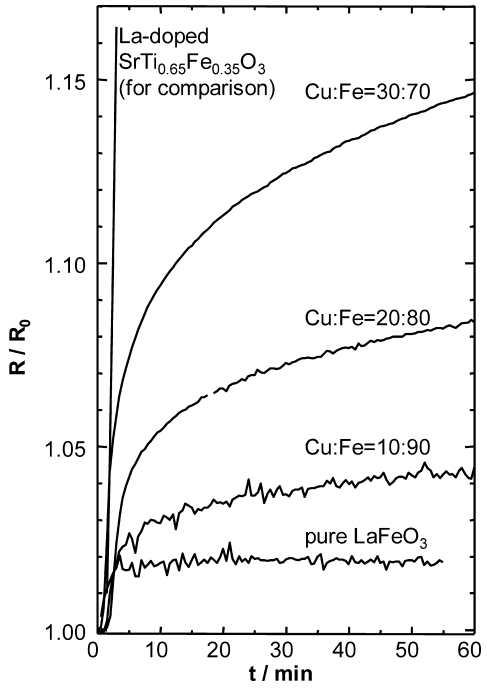

Fig. 1 Sensor deterioration of $LaCu_xFe_{1-x}O_3$ thick films (thickness d approximately 20 μm) according to [15]. For details see text

devices that are exposed to a synthetic exhaust gas containing 3.16 % of oxygen and 40 ppm SO_2[1] at a typical operating temperature of 800°C. As a measure for the deterioration, the effective resistance R at a time t normalized with the resistance $R_0 = R(t = 0)$ is plotted. Material formulations with copper-to-iron-ratios ranging from 10:90 to 30:70 are contrasted to a 5% La-doped $SrTi_{0.65}Fe_{0.35}O_{3-\delta}$ sensor, whose proneness toward sulfur dioxide poisoning is well-known and prevents its unprotected use for oxygen sensing in spite of its excellent temperature independent characteristics [17]. In the above-mentioned study, the resistance of such a $La_{0.05}Sr_{0.95}Ti_{0.65}Fe_{0.35}O_{3-\delta}$ sensor was found to deteriorate rapidly within the first minute of aging, presenting an increase of more than 15%. The devices prepared from $LaCu_xFe_{1-x}O_3$, however, present a sharp, step-like onset at the beginning of sulfur dioxide exposure, followed by a shallow increase. This first step can be attributed to a fast sulfur adsorption and the formation of surface sulfite ions in analogy to the mechanism described in [18] for sulfur dioxide poisoning of $SrTi_{1-y}Fe_yO_{3--\delta}$. The following shallow increase of the sensor resistance might be due to a slow decomposition process.

[1] For comparison: in real exhaust gas, the concentration of sulfur dioxide due to sulfur components in the fuel is less than 10 ppm (conventional fuel with 200 mg/kg sulfur). So-called sulfur-free fuels contain less than 10 mg/kg fuel sulfur, leading to about 0.5 ppm SO_2 in the exhaust at $\lambda = 2$.

With decreasing copper contents, the lifetime of the sensor devices when exposed to sulfur dioxide increases, approaching the excellent stability of pure $LaFeO_3$. Even after 1 hour, the resistance increase that was observed e.g. for the sensor with a copper-to-iron-ratio of 20:80 was lower than 8%.

This contribution focuses on oxygen sensor characteristics of the material system La_2CuO_4-$LaFeO_3$ (denoted as LCxF with x representing the copper ion content as a percentage). LC30F, a member of this material family, has already been successfully investigated as a fast temperature-independent oxygen sensor formulation [19].

After commenting on the poly-phase properties of this p-type conducting system, sensitivity measurements in the high operating temperature range from 650 °C to 900 °C are discussed. In order to obtain a more complete picture of the material properties, densely sintered ceramic specimens are compared to screen-printed thick films. An initial model based on the general effective media theory is developed in order to correlate the copper content x with the oxygen sensitivity.

Experimental

Ball-milled powders of different LCxF-compositions were synthesized from commercially available oxides, i.e. La_2O_3, CuO and Fe_2O_3 powders (all Alfa Aesar, Karlsruhe, Germany, No. 11264, 41692, and 12375, respectively). After calcination at 870°C, the powders were either used to prepare ceramic bulk specimens (sintering temperatures in the range between 1100°C for pure La_2CuO_4 and 1300°C for pure $LaFeO_3$) or to obtain screen-printable pastes (sintering temperature in the range of 975°C for pure La_2CuO_4 and 1100°C for pure $LaFeO_3$). The pastes were printed on conventional alumina substrates.

XRD patterns of LCxF powders are presented in Fig. 2. They clearly indicate the poly-phase structure of the powders, which can be indexed as a mixture of a $LaFeO_3$ and a La_2CuO_4 lattice. In spite of this heterogeneity, the materials could be processed easily for copper contents $x < 60\%$. At higher copper contents, a CuO phase was observed in XRD.

For bulk testing, thin plates (thickness d approximately 600 μm, width w: 4 mm) were prepared from densely sintered specimens. The densities of the specimens were estimated from the SEM cross sections to be over 95% (cf. Fig. 3). Four platinum electrodes were then applied with a brush (spacing l between 2 and 4 mm). In addition to the bulk sensors, thick film sensors were deposited directly on alumina substrates equipped with a set of platinum electrodes (spacing l: 1.1 mm) for electrical contacts. The thick films obtained by screen-printing presented typically a width w of 1 mm and a thickness d between 15 and 25 μm after sintering at 975°C.

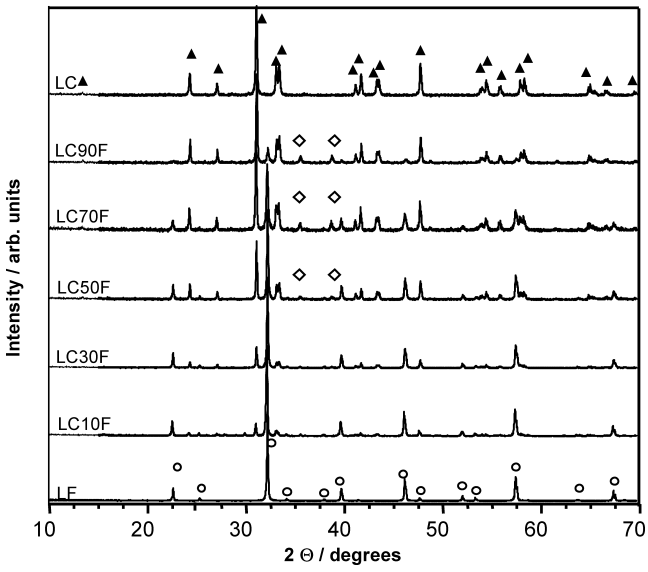

Fig. 2 XRD patterns of LCxF powders. For the sake of clarity, only some of the synthesized LCxF compositions are represented. ▲: La_2CuO_4, 38-0709, ○: $LaFeO_3$, 37-1493, ◇: CuO, 41-0254 (all JCPDS)

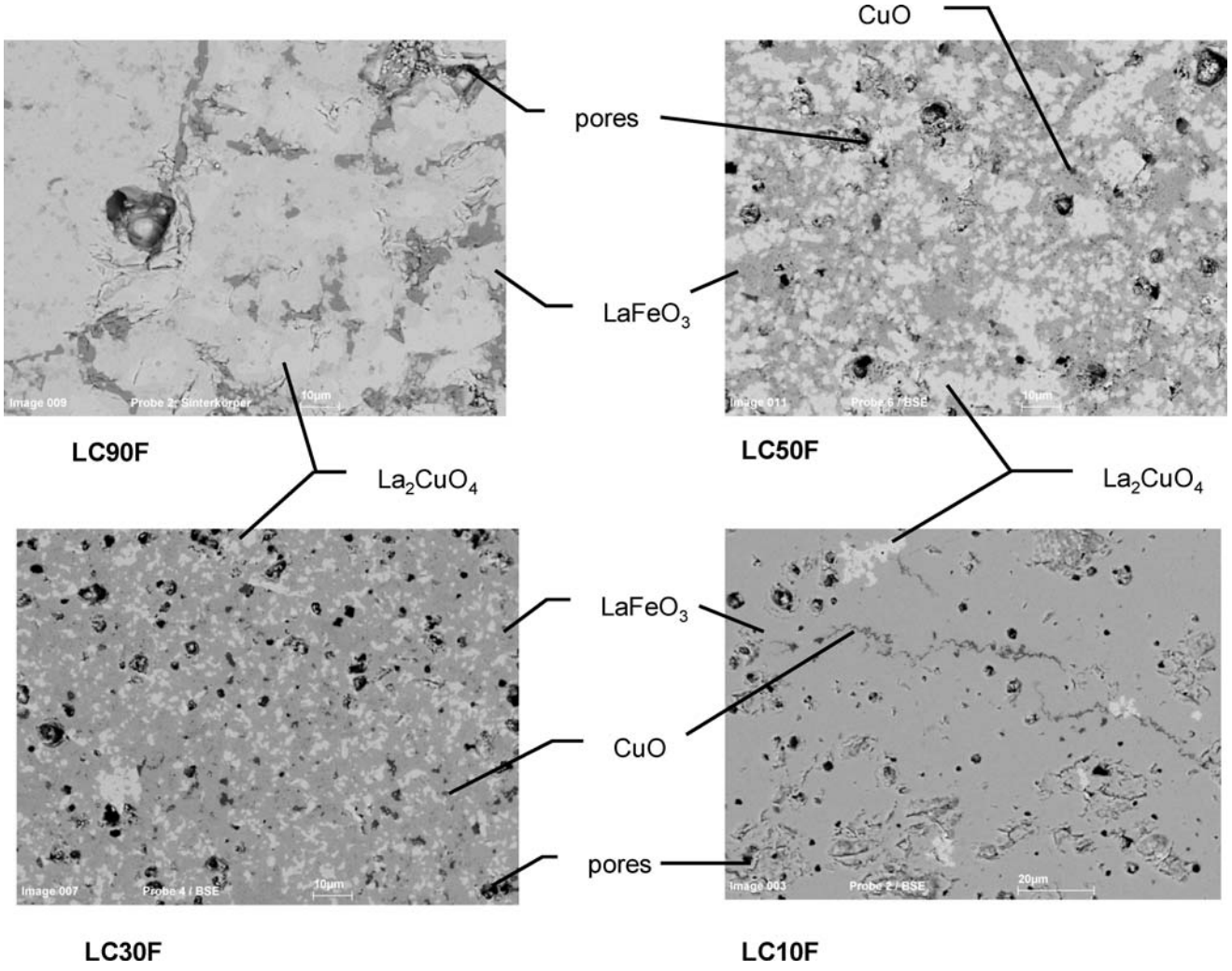

Fig. 3 SEM cross sections of densely sintered LCxF ceramics with an iron-rich phase (dark regions) and a phase rich in copper (clearer regions). The black spots are attributed to a CuO phase. For details: see text

Sensor characteristics of ceramic and thick film specimens were determined in a conventional gas sensor test bench. The sensors were heated in a tube furnace to the appropriate operating temperatures from 650°C to 900°C. To a reference nitrogen flow, O_2 was added using mass flow controllers, leading to O_2 concentrations between 0.1% and 100% ($pO_2 = 10^{-3}$..1 bar). The total gas flow was adjusted to 200 ml/min. In some cases the gas flow was increased to 600 ml/min, in order to exclude a cross interference of the flow rate on the sensor signal. The dc resistance of the samples was measured in conventional 4-probe-technique with a digital multimeter (Keithley 2700). In order to ensure compensation of possible thermo-voltages, the so-called offset-compensation option of the multimeter was enabled. The oxygen concentration was monitored with an amperometric zirconia oxygen sensor (LSU 4.7, ETAS, Germany). In addition, a paramagnetic O_2-detector (Fisher Rosemount, NGA 2000) was used for spot-checks of the oxygen concentration.

Results and discussion

Figure 3 shows cross section SEM micrographs of samples prepared from densely sintered LCxF ceramics. One can readily distinguish between an iron-rich phase (dark regions) and a phase rich in copper (clearer regions). Using EDX measurements, both phases were clearly identified as $LaFeO_3$ and La_2CuO_4, respectively. In addition, the presence of the CuO phase (black spots in the SEM micrographs) for high cooper contents was confirmed. Hence, the EDX observations from the ceramic specimens are in agreement with the XRD results of the starting powders. It is therefore concluded that sintering at high temperatures did not affect the phase composition.

In Fig. 4(a), the results of an oxygen sensitivity test at 750 °C are presented exemplarily for a thick film sensor and a ceramic specimen prepared of the LC30F composition. The resistance traces indicate a fast response time of the thick film

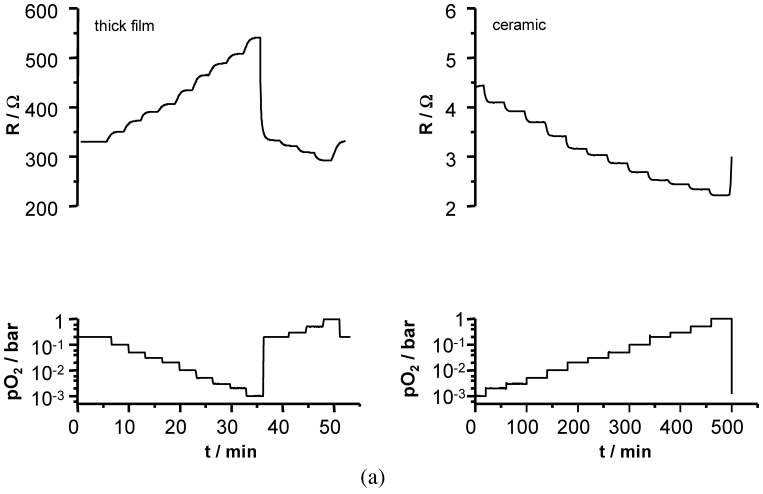

Fig. 4(a) Resistance traces of LC30F thick film (left) and ceramic specimens (right). Operating temperature: 750°C. Note the different scaling of the abscissae,

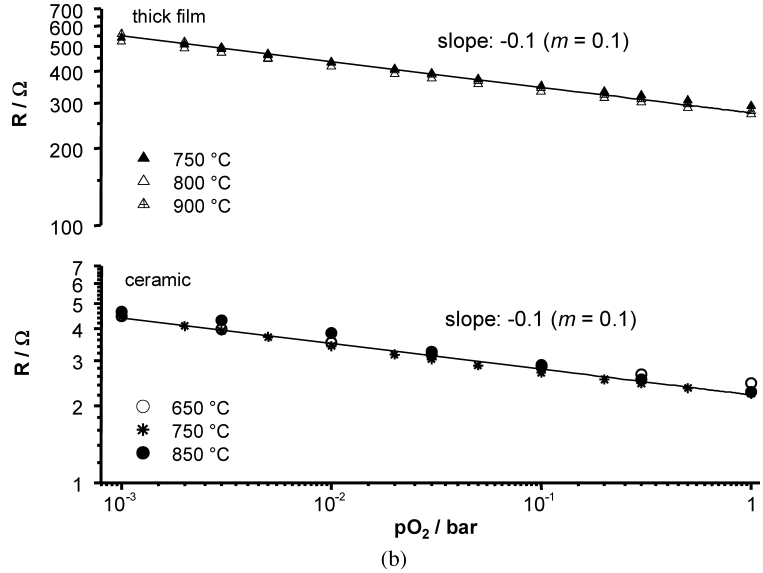

Fig. 4(b) Oxygen sensitivity of LC30F thick film (upper part) and ceramic specimens (lower part). Operating temperatures as indicated

in the range of a few seconds, limited by the settling time of the test bench, whereas the response time of the densely sintered specimen is somewhat higher (in the range of minutes). The fast response of the LC30F thick films has been verified and discussed in a previous study [19]. From defect chemical models, the general correlation between the resistance R of an oxide ceramic and the oxygen partial pressure pO_2 is given by Eq. (1)

$$R = R_0 \cdot \exp\left(\frac{E_A}{kT}\right) \cdot pO_2^{-m} \tag{1}$$

The exponential term stems from the fact that the conductivity σ of semiconductors is thermally activated, following an Arrhenius-type behavior with the activation energy E_A. In order to evaluate the oxygen sensitivity of the samples, one generally uses the slope m of the double-logarithmic representation $\lg(R)$ vs. $\lg(pO_2)$ at one specific temperature T, which is represented in Fig. 4(b) for the LC30F composition for various operating temperatures between 650°C and 900°C.

Both thick film and ceramic specimen show an identical slope m in the double-logarithmic representation. This good correlation was observed for each tested LCxF composition. In addition, the LC30F composition clearly presents a temperature-independent behavior, which is in agreement with the former results [19].

In order to identify the most suitable compositions for temperature-independent oxygen sensing, all materials were characterized in the temperature range from 650°C to 900°C with respect to oxygen sensitivity and temperature dependency.

In Fig. 5, the slope m determined from oxygen sensitivity plots as shown previously is given as a function of the copper content x. Exemplarily, data points are shown for operating temperatures of 750°C for the ceramics and of 750°C and 800 °C for the thick film samples.

As a measure for temperature dependency, the thermal activation energy E_A is used as defined in Eq. (1). The closer E_A is to zero, the less temperature-dependent is the material.

Figure 6 shows the values of E_A in air as a function of x, which are calculated from the slopes of the Arrhenius representation $\ln(R)$ vs. $1/T$.

The oxygen sensitivity of the LCxF compositions increases steadily with the copper content from values of about $m = 0.02$ for pure lanthanum ferrate ($x = 0$) to $m = 0.18$ for pure lanthanum cuprate ($x = 100\%$). At the same time, one observes a perfect temperature independency for $x > 30\%$ in the case of the thick films. For the bulk ceramics, temperature independency begins at even lower copper contents ($x > 20\%$). This behavior strongly hints that oxygen sensitivity of the system is governed by the lanthanum cuprate phase. Lanthanum ferrate could be considered as a matrix, which is expected to improve the poor thermal and chemical stability of the pure lanthanum cuprate.

According to these observations, an initial model based on the generalized effective media theory (GEMT) was adopted in order to describe the properties of the composite LCxF, which is considered here as a bi-phase material. This theory, which has been developed from the so-called percolation theory and the effective media theory (see e.g. review [21]), was introduced for predicting the global properties of polymer matrices containing different kinds of filler particles [22]. Eq. (2) describes the resulting conductivity σ_{res} of such a bi-phased system [23].

$$\frac{(1-\phi)\left(\sigma_m^{1/t} - \sigma_{res}^{1/t}\right)}{\sigma_m^{1/t} + \frac{1-\phi_c}{\phi_c}\sigma_{res}^{1/t}} + \frac{\phi\left(\sigma_f^{1/t} - \sigma_{res}^{1/t}\right)}{\sigma_f^{1/t} + \frac{1-\phi_c}{\phi_c}\sigma_{res}^{1/t}} = 0. \tag{2}$$

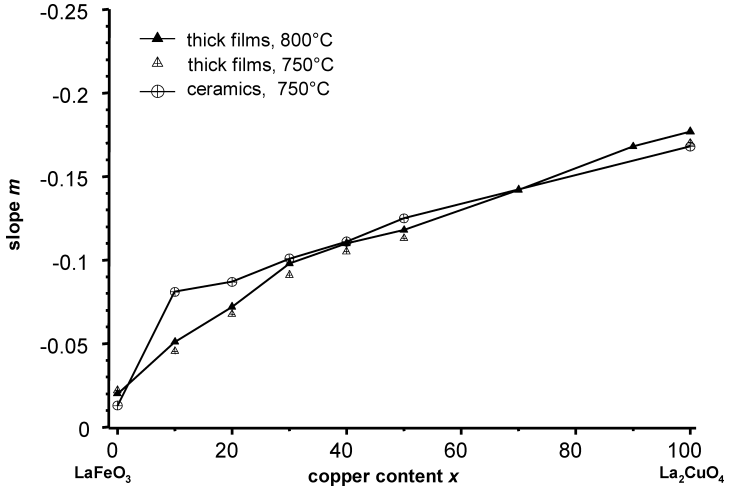

Fig. 5 Oxygen sensitivity for thick films and ceramics as a function of the copper content x. Operating temperature as indicated

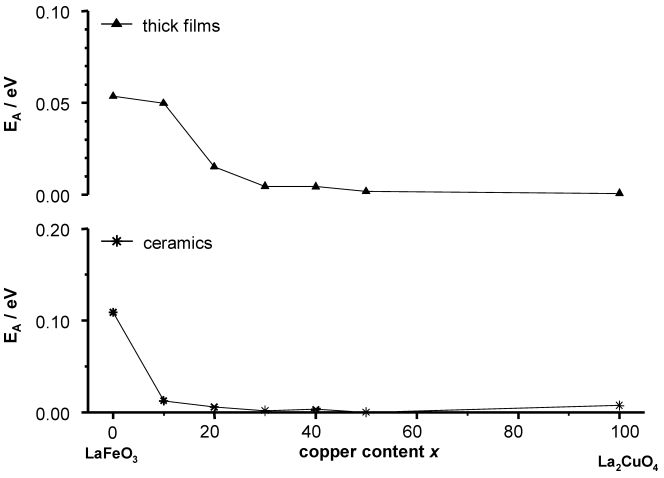

Fig. 6 Thermal activation energy E_A according to Eq. (1) for thick films (upper part) and ceramics (lower part)

Here, σ_m and σ_f denote the conductivity of matrix and filler, ϕ is the volume fraction of the filler phase, ϕ_c and t are fit parameters. The fit parameter t includes the different temperature dependency of matrix and filler as well as the different aspect ratios and distributions of the single material phases.

The parameter ϕ_c in Eq. (2) is commonly interpreted as the percolation threshold, i.e. the critical volume fraction of filler particles leading to a closed filler network in the surrounding matrix [24]. Assuming that $\sigma_f > \sigma_m$, the properties of the composite are mainly determined by the filler properties if $\phi > \phi_c$. Else, the system is governed by the matrix. One of the starting-points of the GEMT, the so-called percolation theory (PT), is only valid for σ_f tending toward infinity and $\sigma_m = 0$. This scenario corresponds to a perfect conductor distributed in a perfectly insulating matrix [24, 25]. As a consequence, PT only covers the composition range above the percolation threshold $\phi > \phi_c$. For $\phi < \phi_c$, no conductive path exists, and the overall conductivity of the composite equals zero in the PT.

In contrast, the GEMT describes the composite properties for finite conductivities, thus covering the entire composition range $0 \leq \phi \leq 1$. Furthermore, the GEMT allows for different aspect ratios and distributions of the filler by introducing the parameter t [22, 26].

In the present study, Eq. (2) was used to fit the experimental data of oxygen sensitivity measurements on LCxF with the technical computing software Matlab according to a least square fit. In a first approach, only the data for copper contents $x \leq 50\%$ is considered in order to justify the assumption of a two-phase composite. The presence of a third CuO phase detected by XRD and EDX measurements at higher copper contents is thus not taken into account. For the fitting procedure, the volume fraction ϕ was calculated from the molar fraction $\zeta = x/100\%$ according to Eq. (3).

$$\frac{\frac{\zeta \cdot M_{LC}}{2 \cdot \rho_{LC}}}{\frac{\zeta \cdot M_{LC}}{2 \cdot \rho_{LC}} + (1-\zeta)\frac{M_{LF}}{\rho_{LF}}} = \phi. \tag{3}$$

M_{LC} and ρ_{LC} are the molecular weight and the density of pure La_2CuO_4, respectively. M_{LF} and ρ_{LF} denote the molecular weight and the density of pure $LaFeO_3$. This equation allows for the fact that the molar fractions $\zeta = x/100\%$ is based on the initial net weight of the educts CuO and Fe_2O_3.

In Fig. 7, the results of such a fit for LCxF ceramics and thick films in air and for $pO_2 = 0.002$ bar are represented exemplarily (lines). From the experimental resistance data R obtained at 800°C (thick films) and 750°C (ceramics), the conductivity σ of the specimens was calculated using Eq. (4)

$$\sigma = \frac{1}{R} \cdot \frac{w \cdot d}{l} \tag{4}$$

where l is the electrode spacing, w the width and d the thickness of the sample. The experimentally obtained conductivity points are plotted as symbols.

As fit parameter pairs, $\phi_c = 0.08$ (corresponding to $x = 10\%$), $t = 0.1067$ ($pO_2 = 0.2$ bar), and $t = 0.0397$ ($pO_2 = 0.002$ bar) were used for the ceramic sample. In the case of the thick film, the corresponding parameter pairs were $\phi_c = 0.05$ (corresponding to $x = 6.43\%$), $t = 0.75$ ($pO_2 = 0.2$ bar), and $t = 0.502$ ($pO_2 = 0.002$ bar), respectively. The values of σ_f and σ_m were taken from experimental results of pure La_2CuO_4 and $LaFeO_3$.

The experimental data is fitted well even by this un-refined initial model without taking into account the presence of a third phase or the porosity of the samples. One notable difference between the ceramics and the thick film specimens is the steepness of the conductivity increase. In the case of the densely sintered ceramics, the conductivity curve presents a clear percolation-like behavior with a sharp increase at one specific copper content $x = 10\%$. For the porous thick films, however, the curve shape is much shallower, and the percolation threshold is somewhat blurred. As a consequence, the fitted value of ϕ_c (and the corresponding x) is lower compared to the dense ceramics. An explanation of this observation is that the present model has been developed for a bi-phase ma-

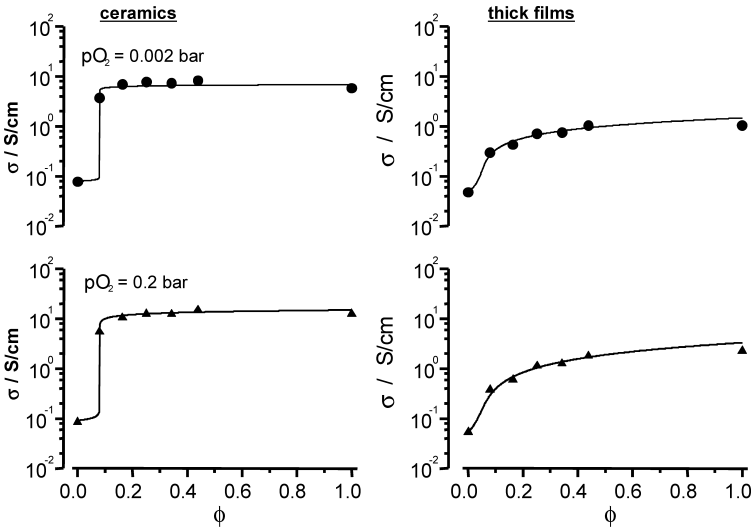

Fig. 7 Theoretical (lines) and experimental (symbols) conductivity data of ceramics (left, $T = 750$°C) and thick films (right, $T = 800$°C). Oxygen partial pressure as indicated. For details see text

terial. While this assumption still holds for the LCxF bulk ceramics, it merely serves as a rough approximation for the porous thick films. In the case of the latter, the porosity of the samples should be taken into account to determine more meaningful values for the percolation threshold ϕ_c.

The present model is then used to predict the slope values m as a function of the copper content x for the thick film devices. The modeling was conducted according to the following process. Considering the physical meaning of the fit parameters ϕ_c and t, the critical volume fraction ϕ_c should not depend on the oxygen partial pressure pO_2. Therefore, a fixed value $\phi_{c,fix} = 0.05$ is chosen based on the preliminary results. A corresponding parameter set $t(pO_2)$ is then determined by fitting the experimental data obtained for each oxygen concentration. Finally, the theoretical conductivity values $\sigma_{res}(pO_2)$ are calculated for each LCxF composition using the corresponding parameter set $(\phi_{c,fix}, t(pO_2))$. Calculated and experimentally obtained curves are shown in Fig. 8. In Table 1, the corresponding slope values are compared.

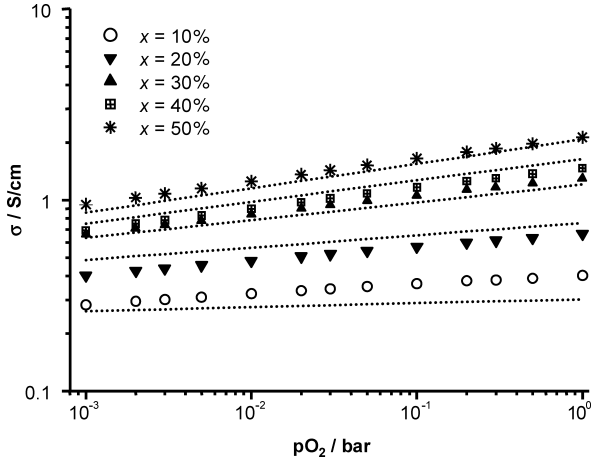

Fig. 8 Theoretical (lines) and experimental (symbols) oxygen sensor characteristics in a double-logarithmic representation

Table 1 Calculated and experimentally obtained slope values m as a function of the material composition

	Cu content x/%	10	20	30	40	50
slope value m	experimental	0.05	0.07	0.098	0.11	0.12
	calculated	0.02	0.065	0.093	0.11	0.13

The obtained results are very promising, given that the un-refined initial model already leads to a very good approximation of the actual oxygen sensing characteristics.

A more careful adjustment of the model should enable to even better predict the slope values m as a function of the copper content x. In particular, the influence of the oxygen partial pressure on the parameter t needs to be studied further in order to understand its physical meaning more in detail. Furthermore, a more complete model should also take into account the porosity of the thick films as well as the presence of the CuO phase, which has not been considered here as $x \leq 50\%$. Ongoing studies are also aiming at investigating the temperature dependency of the parameter t to allow for the fact that a perfect temperature independency is only observed for $x > 30\%$. Thus, the present model is going to be refined in order to describe the material system more exactly.

Conclusion

In spite of its poly-phase microstructure, the material family lanthanum cuprate—lanthanum ferrate was shown to present promising oxygen sensor characteristics. In particular, one obtains temperature-independent devices at low copper con-

tents, thus combining the advantages of pure lanthanum cuprate with the sulfur stability of the lanthanum ferrate.

A model based on the generalized effective media theory was successfully adopted to correlate the gas sensor behavior and the material composition. Initial calculations allow to fit the actual sensor characteristics satisfyingly. By further investigating the properties of the fit parameter t and by allowing the presence of a third phase such as pores, the model can be expanded to the entire temperature range, which is valuable for materials development.

Furthermore, more careful studies of long term thermal and chemical stability need to be conducted in the future. In particular, phase stability of the poly-phase microstructure at high temperatures needs to be confirmed. Although sulfur stability has been addressed in a previous study, stability data in reducing atmospheres are still missing.

Acknowledgements The authors gratefully acknowledge the work of Mrs. M. Wickles, Mr. P. Kostolansky, and Mr. J. Deerberg (all University of Bayreuth), for sample preparation, XRD and SEM studies.

References

1. H. Wiedenmann, G. Hötzel, H. Neumann, J. Riegel, F. Stanglmeier, and H. Weyl, *Exhaust Gas Sensors*, in Automotive Electronics Handbook, 2nd edition, R. Jurgen(Ed.), Mc Graw-Hill, New York, 6.1–6.25 (1999).
2. A. Takami, "Development of titania heated exhaust-gas oxygen sensor," *Ceram. Bull.*, **67**, 1956–1960 (1988).
3. J. Gerblinger, M. Hauser, and H. Meixner, "Electric and kinetic properties of screen-printed strontium titanate films at high temperatures," *J. Am. Ceram. Soc.*, **78**, 1451–1456 (1995).
4. N. Izu, W. Shin, I. Matsubara, and N. Murayama, "The effects of the particle size and crystallite size on the response time for resistive oxygen gas sensor using cerium oxide thick film," *Sens. Actuators B*, **94**, 222–227 (2003).
5. N. Izu, W. Shin, and N. Murayama, "Fast response of resistive-type oxygen gas sensors based on nano-sized ceria powder," *Sens. Actuators B*, **93**, 449–453 (2003).
6. J. Gerblinger, H. Meixner, and P. Kleinschmidt, "Rapid, temperature-compensated sensor, in particular for oxygen and automobile exhaust fumes," WO 90/03569 (1990).
7. J. Gerblinger and H. Meixner, "Device for determining the partial pressure of gases in a gas mixture," European Patent Application EP 563613 A2 (1993).
8. N. Izu, W. Shin, I. Matsubara, and N. Murayama, "Small temperature-dependent resistive oxygen gas sensor using $Ce_{0.9}Y_{0.1}O_{2-\delta}$ as a new temperature compensating material," *Sens. Actuators B*, **101**, 381–386 (2004).
9. P. Moseley and D. Williams, "Gas sensors based on oxides of early transition metals," *Polyhedron*, **8**, 1615–1618 (1989).
10. R. Moos, W. Menesklou, H. Schreiner, and K.H. Härdtl, "Materials for temperature independent resistive oxygen sensors for combustion exhaust gas control," *Sens. Actuators B*, **67**, 178–183 (2000).
11. R. Moos, F. Rettig, A. Hürland, and C. Plog, "Temperature-independent resistive oxygen exhaust gas sensors for lean-burn engines in thick-film technology," *Sens. Actuators B*, **93**, 42–49 (2003).
12. R. Blase, K. Härdtl, U. Schönauer, "Oxygen Sensor based on non-doped cuprate," United States Patent Specification, US 5,792,666 (1997).
13. R. Blase and K. Härdtl, "Schneller Sauerstoffsensor zur Regelung von Verbrennungsvorgängen" (Fast Oxygen Sensor for Combustion Control), in: VDI-Berichte 1255, VDI-Verlag Düsseldorf, Proceedings of "Sensoren und Messysteme", Bad Nauheim, Germany, 11–13 March 1996, 137–142 (1996).
14. A. Krug, "(La,Sr)FeO_3—Elektrische Eigenschaften und Sensoranwendungen ((La,Sr)FeO_3-Electrical properties and sensor applications)," Ph.D. thesis, Universität Fridericiana Karlsruhe, Karlsruhe, Germany, (1994).
15. R. Moos and F. Rettig, "Resistiver Sauerstoffsensor (Resistive Oxygen Sensor)," German Patent Specification, DE10114645C1 (2003).
16. F. Rettig, R. Moos, and C. Plog, "Novel temperature independent resistive oxygen sensor without sulfur instability for combustion engine exhaust," Sensor 2003 Proceedings, Nürnberg, Germany, 13–15 May 2003, 277–282 (2003).
17. F. Rettig, R. Moos, and C. Plog, "Sulfur adsorber for thick-film exhaust gas sensors," *Sens. Actuators B*, **93**, 36–41 (2003).
18. F. Rettig, R. Moos, and C. Plog, "Poisoning of temperature independent resistive oxygen sensors by sulfur dioxide," *J. Electroceram.*, **13**, 733–738 (2004).
19. K. Sahner, R. Moos, N. Izu, W. Shin, and N. Murayama, "Resistive temperature-independent oxygen sensors: a comparative study," *Sens. Actuators B*, **113**, 112–119 (2006).
20. K. Sahner, R. Moos, M. Matam, J. Tunney, and M. Post, "Hydrocarbon sensing with thick and thin film p-type conducting perovskite materials," *Sens. Actuators B*, **108**, 102–112 (2005).
21. R. Landauer, *Electrical Conductivity in Inhomogeneous Media*(Edited by), D. T. J.C. Garland, American Institute of Physics, New York, 2–45 (1978).
22. D.S. McLachlan, "An equation for the conductivity of binary mixtures with anisotropic grain structures," *J. Phys. C: Solid State Phys.*, **20**, 865–877 (1987).
23. R.H. Cruz-Estrada and M.J. Folkes, "Structure formation and modelling of the electrical conductivity in SBS-polyaniline blends. Part II Generalized effective media theories approach, *Journal of Materials Science Letters*," **21**, 1431–1434 (2002).
24. D.S. McLachlan, "Measurement and analysis of a model dual-conductivity medium using a generalised effective-medium-theory," *J. Phys. C: Solid State Phys.*, **21**, 1521–1532 (1988).
25. R.H. Cruz-Estrada and M.J. Folkes, "Structure formation and modelling of the electrical conductivity in SBS-polyaniline blends. Part I Percolation theory approach," *Journal of Materials Science Letters*, **21**, 1427–1429 (2002).
26. D.S. McLachlan, M. Blaszkiewicz, and R.E. Newnham, "Electrical resistivity of composites," *J. Am. Ceram. Soc.*, **73**, 2187–2203 (1990).